

Optical simulations of gravitational effects in the Newton–Schrödinger system

Rivka Bekenstein^{*}, Ran Schley, Maor Mutzafi, Carmel Rotschild and Mordechai Segev

Some predictions of Einstein's theory of general relativity (GR) still elude observation, hence analogous systems, such as optical set-ups, have been suggested as platforms for emulating GR phenomena. GR is inherently nonlinear: for example, the curvature of space is induced by masses whose dynamics is also affected by the curved space they themselves induce. But, thus far all GR emulation experiments with optical systems have reproduced only linear dynamics. Here, we study gravitational effects with optical wavepackets under a long-range nonlocal thermal nonlinearity. This system is mathematically equivalent to the Newton–Schrödinger model proposed to describe the gravitational self-interaction of quantum wavepackets. We emulate gravitational phenomena by creating interactions between a wavepacket and the gravitational potential of a massive star, observing gravitational lensing, tidal forces and gravitational redshift and blueshift. These wavepackets interact in the curved space they themselves induce, exhibiting complex nonlinear dynamics arising from the interplay between diffraction, interference and the emulated gravitational effects.

Emulating GR phenomena¹ in laboratory experiments aims to study the dynamics of light and masses in curved space. Such experimental settings enable control over physical parameters, suggest new insights and offer considerable intuition. Among other settings^{2–4}, table-top optical experiments^{5–11} play a major role. Initiated by the discovery that moving media act as gravitational fields on light^{5,6}, these ideas led to the demonstration of an event horizon by using ultra-short optical pulses⁸. Likewise, it has been shown¹¹ that engineering the refractive index structure can mimic gravitational lensing^{9–11}. Other studies explored wave dynamics in curved space, by coating a three-dimensional body with a waveguiding layer confining the light to propagate within it, obeying a wave equation in curved space^{12–14}. Interestingly, the dynamics of optical wavepackets in curved space can strongly differ from that of particles, as the wavefunctions do not necessarily propagate along shortest paths (geodesic lines)¹⁴. Some of the studies emulating GR effects included optically nonlinear effects^{8,14–17}, such as solitons¹⁶, nonlinear accelerating beams¹⁴, and event horizon induced by another (powerful) wave in a pump–probe experiment⁸. However, thus far in all experimental work on this topic^{8–11} the curved space is acting on the probed beam in a linear manner: the space curvature is always fabricated—via metamaterials^{18,19} or controlled by pump beams⁸—not revealing the actual nonlinear dynamics of GR. Importantly, all of these studies employed local optical nonlinearities, such as the Kerr effect or saturable Kerr-like nonlinearity^{8,14,16}, whereas long-range dynamics is inherent in many GR phenomena^{20–22}. As we show below, a nonlocal nonlinearity is a natural setting for studying long-range GR effects^{23–25}, such as tidal forces in the vicinity of stars and gravitational lensing. Such gravitational phenomena—when emulated by static optically nonlinear systems—necessitate a highly nonlocal nonlinearity. The dynamics of an optical wavepacket in the presence of the highly nonlocal thermal optical nonlinearity is described by two coupled equations²⁴: the paraxial wave equation, which is mathematically equivalent to the Schrödinger equation in two transverse dimensions and time (so-called 2D+1) (which was extensively used for observing many fundamental phenomena^{26–30}) and the Poisson (Newton-type) equation, describing the dependence of the refractive index on the

light intensity. This set of equations is mathematically equivalent to the 2D+1 Newton–Schrödinger model (NSE; refs 31–39). The NSE describes a quantum mass density evolving according to the Schrödinger equation in the presence of a gravitational potential created by the mass density itself, specifically for the non-relativistic limit of the Klein–Gordon (or Dirac) wavefunctions. The NSE is used as a phenomenological model describing the gravitational self-interaction of a condensate in the Hartree approximation (mean-field many-body system)^{32,37–39}. Although the NSE does present differences from GR, it nonetheless describes self-interaction, in the spirit of Einstein's statement on GR: 'The geometrical states of bodies and the rates of clocks depend in the first place on their gravitational fields, which again are produced by the material systems concerned'⁴⁰. The NSE model is attracting considerable interest in the GR community because, in the absence of a unified theory of gravitation and quantum fields—as is the state of the art today—this model can considerably contribute to the intuition and understanding. Also, it was suggested that the NSE can model the gravitational self-interaction of a non-relativistic quantum particle, which can in principle question the necessity of quantum gravity⁴¹.

Thus far, however, the NSE has been studied strictly theoretically^{31,32,36}, because the gravitational potential in quantum mechanical systems is extremely weak, making the NSE still inaccessible to laboratory experiments. It is therefore very interesting to exploit the analogy between the NSE dynamics and the propagation of optical wavepackets in the presence of a highly nonlocal thermal optical nonlinearity, to study the effects of gravitational phenomena on wavepackets in the NSE framework. Naturally, the ability to explore the NSE system in experiments raises numerous intriguing questions: How does the dynamics of structured wavepackets differ from that of Gaussian wavepackets under the NSE model? How would the long-range nonlinearity affect the structure and the evolution of the wavepackets? Is it possible to observe GR phenomena, such as tidal forces, in this NSE framework, and can interference phenomena overcome gravitational effects?

Here, we study the interaction between optical wavepackets in the presence of a thermal optical nonlinearity, which is governed by the NSE model. These wavepackets are analogous to quantum

wavefunctions under the influence of gravitational fields that they themselves induce—creating mutual nonlinear dynamics. Specifically, we study the evolution of a broad accelerating wavepacket interacting with an intense Gaussian beam that creates a gravitational potential equivalent to that of a massive body. We observe gravitational lensing and tidal forces that act on the wavepackets, giving rise to complex dynamics involving interference and diffraction that depend on the intensity of the beams (equivalent to the mass density in the NSE frame). We use specific wavepackets to study the interplay between diffraction and gravitational dynamics, and exploit the bending of accelerating wavepackets towards a star (or outwards from it) to demonstrate gravitational blueshift (or redshift).

We begin by describing our system. Light propagating through a slightly absorbing medium acts as a heat source. The heat diffuses according to the heat equation, giving rise to a temperature change everywhere in the bulk, all the way to the boundaries (which are held at constant temperature). This creates a non-uniform temperature distribution in the medium, which in turn modifies the refractive index at every point. In some materials, such as lead glass, the refractive index increases with the temperature, which yields a high self-focusing effect. This thermal nonlinearity can support nonlocal solitons^{23,24} which exhibit interactions from very far away²⁵. The relation between the heat source (beam intensity) and the change in the refractive index is given by a Poisson equation:

$$\frac{\kappa}{\beta} \nabla^2 \Delta n = -\alpha |\psi|^2 \tag{1}$$

Here, β describes the dependence of the change in the refractive index on the temperature change ($\Delta n = \beta \Delta T$), κ is the thermal conductivity, α is the linear absorption coefficient of the material, and ψ is the slowly varying amplitude of the EM wave. Specifically in lead glass, the thermal nonlinearity is strong, even though the absorption is weak and can be safely neglected for large propagation distances²⁴. The evolution of the slowly varying envelope $\psi(x, y, z)$ is described by the nonlinear paraxial equation:

$$i\psi_z + \frac{1}{2k} \nabla_{\perp}^2 \psi + \frac{k\Delta n}{n_0} \psi = 0 \tag{2}$$

The coupled equations (1) and (2) describe the propagation of the light in a medium exhibiting the thermal nonlinearity (k is the wavenumber, and n_0 is the ambient refractive index). In the paraxial regime, the Laplacian in the equation (1) is only two-dimensional (x, y) because the variations of the dynamics in z are small compared with those in the transverse directions (see Supplementary Information). Equations (1) and (2) stand in a complete mathematical analogy with the 2D+1 Newton–Schrödinger equations:

$$\begin{aligned} \nabla_{\perp}^2 \phi &= 4\pi G m |\psi|^2 \\ i\hbar\psi_t + \frac{\hbar^2}{2m} \nabla_{\perp}^2 \psi - m\phi\psi &= 0 \end{aligned} \tag{3}$$

The Newton equation is a Poisson equation for the gravitational potential ϕ , with the mass density $m|\psi|^2$ acting as a source term, where G is that gravitational constant. The dynamics of the quantum wavefunction (ψ) is therefore described by the Schrödinger equation with a gravitational potential generated by its mass density. In our optical system, the propagation direction z plays the role of time, hence the dynamics described by the time-dependent Schrödinger equation can be studied in our optical set-up by examining the spatial evolution (of time-harmonic fields) along the propagation direction (z). Throughout this article, we use accelerating beams as a means to study the curved space dynamics of wavepackets in the vicinity of massive objects. It is therefore essential to recall basic concepts of accelerating beams. Accelerating wavepackets were

first proposed in quantum mechanics⁴², and three decades later were introduced into optics^{43,44}, where they are having a major impact^{45,46}. In their spatial paraxial manifestation, these are Airy beams propagating along parabolic trajectories while maintaining their shape owing to linear interference effects caused by their unique structure. We chose accelerating beams specifically because, in the absence of nonlinearity, they are shape-preserving. As such, they enable the observation of emulated gravitational effects caused by the interaction, without being overshadowed by spatial diffraction-broadening. Also, accelerating beams have a broad structure which enables clear demonstration of the gravitational effects, while at the same time they have a well-defined peak, whose trajectory plays an important role in systems with interaction^{45–48}. Accelerating beams are expected to have complex dynamics in the presence of nonlocal nonlinearity⁴⁹ because the evolution of their wavefunctions follows non-geodesic trajectories that depend directly on their structure. Hence, the nonlocal nonlinearity may affect both their structure and their trajectory. Their behaviour differs strongly from that of localized particle, and as such it enables the demonstration of the actual wave dynamics of the wavepackets.

In our experimental system (Fig. 1a), an accelerating beam interacts with an intense beam in lead glass, with the interaction being described by equations (1) and (2). The intense beam (emulating a star) is a Gaussian beam of 50 μm FWHM (full-width at half-maximum), which at 1 Watt of power becomes a soliton²⁴. This beam is launched into a lead glass (SF11) sample, of dimensions 4 \times 4 \times 20 mm, at the exact centre of the input facet (xy plane), to ensure propagation parallel to the z axis⁵⁰. The accelerating beam is a two-dimensional (2D) Airy beam, created by a cubic phase mask in k -space. The beams interact with one another from afar inside the glass sample, as the refractive index change induced by the beams extends—following equation (1)—all the way to the sample boundaries. The interaction strength is controlled by varying the laser power, which controls the power of both beams while maintaining their relative power. By imaging the entrance and the exit facets, we monitor the spatial dynamics of the beams. For example, Fig. 1b shows a photograph of the beams as they exit the nonlinear material. Figure 1b shows schematically the trajectories of the 2D Airy beam and of the intense beam inside the sample. In the NSE framework, this scheme is analogous to a broad quantum wavefunction interacting with a more massive body that exerts a gravitational potential on the wavefunction. The unique Airy shape enables experiments to study what happens when the wavepacket is accelerating towards the star or outwards from the star, as shown schematically by the beam trajectories in Fig. 1b. Here, a proper choice of the initial waveform can make the beam overcome the gravitational lensing, and escape from the attraction of the ‘star’ (blue trajectory in Fig. 1b). This happens when the beam is structured with a profile that causes acceleration opposite to the direction of the centre of the potential. Later on, we explain how the nonlocal nonlinear interaction can—counterintuitively—also support that opposite acceleration. Typical results showing measurements of the gravitational lensing are given in Fig. 1c,d. The most pronounced effect is that, as the strength of the interaction increases, the ‘escaping beam’ is attracted more towards the star (green trajectory in Fig. 1b). Monitoring the trajectory of the Airy beam and the shift of its main lobe (Fig. 1c,d) reveals that the attraction towards the centre of the potential grows as the power (of both the ‘star’ and accelerating beam) is increased. Namely, the nonlinear interaction (equivalent to the gravitational lensing) reduces the acceleration of the wavepacket escaping from the vicinity of the star. Surprisingly, for high enough power, the change in the trajectory due to the nonlinearly induced potential saturates (see Fig. 1d).

The saturation effect raises natural questions about its origins. Intuitively, we would expect the shift of the main lobe to increase as the gravitational potential grows, without saturating. This is because our intuition is based on the motion of a localized particle, and a

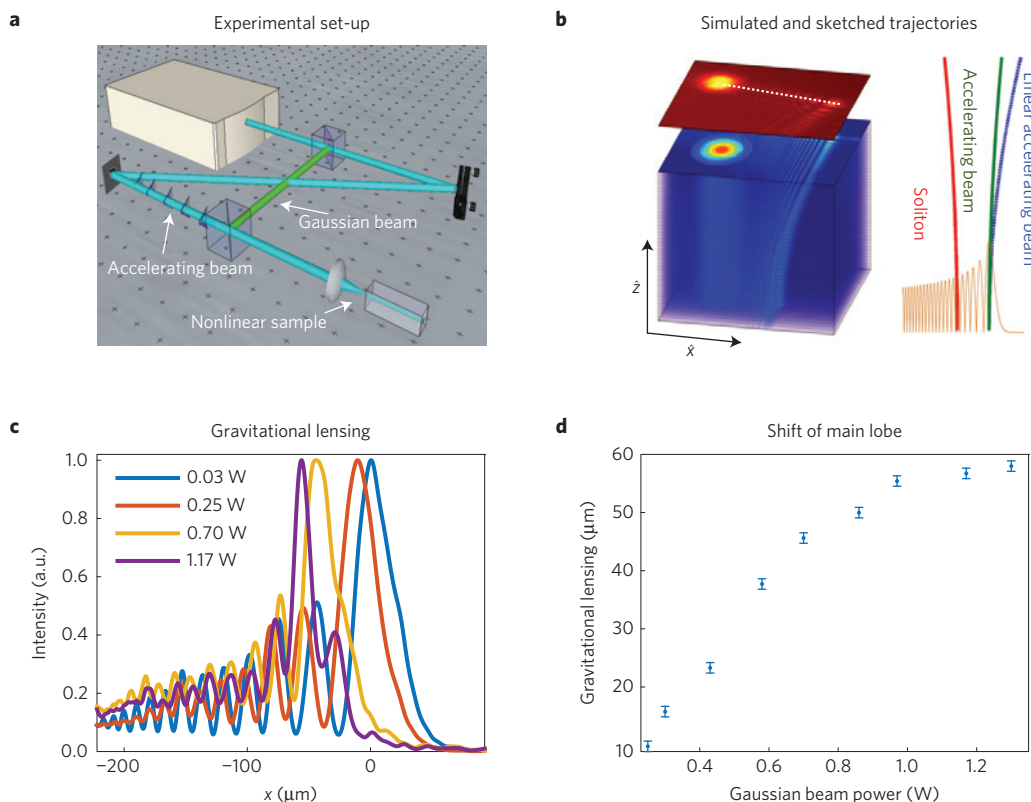


Figure 1 | Experimental settings and results. **a**, A laser beam of 488 nm wavelength is split into a Gaussian beam and a 2D accelerating beam, launched to interact inside a sample of a highly nonlocal nonlinear medium. **b**, Left: simulations showing the dynamics of the powerful beam ('star') and of the accelerating beam in the nonlinear medium (bottom) and photograph of the beams exiting the nonlinear medium (top). Right: schematic top-view sketch of the accelerating beam interacting with the 'star', in the linear (blue curve) and the nonlinear (green curve) regimes. Note that the nonlinear dynamics is mutual: the soliton (red curve) affects the beam accelerating towards it, and at the same time its own trajectory is affected (becomes curved leftwards) by the accelerating beam. **c**, Experimentally measured 1D cross-sections of the accelerating beam taken along the line marked in **b**, for various power levels of the localized beam (various values of the mass of the star). As the power is increased, the main lobe is shifted more strongly towards the powerful beam, in equivalence to gravitational lensing bending light towards a star. **d**, Shift of the main lobe (gravitational lensing) as a function of the power of the Gaussian beam. Note the saturation effect in the shift, reflecting the mutual nonlinear action between the star and the beam accelerating towards it. The vertical error bars indicate the measurement resolution (see Supplementary Information for details regarding data analysis).

linear gravitational potential that is not affected by the presence of the particle. To gain understanding about the nonlinear dynamics in our system, we simulate numerically the propagation dynamics of our launched beams, solving equations (1) and (2) together. The simulations reveal that the gravitational potential of the 'star' not only affects the accelerating beam, but that the accelerating beam also affects the evolution of the 'star'. Interestingly, the combination of the two beams gives rise to a refractive index distribution that is asymmetric with respect to the 'star': it is steeper on the side of the main lobe, which makes the 'star' move away from the main lobe (of the escaping beam) as the interaction strength is increased (see Supplementary Information). The 'star' is shifted away from the main lobe towards the tail of the accelerating beam, which actually contains a considerable fraction of the total beam power. As the power is increased, the attractive force exerted by the 'star' on the main lobe weakens, owing to a decrease in the slope of the potential in the region of the accelerating beam. Thus, the refractive index structure during the high-power interaction affects the gravitational lensing of the main lobe—creating a saturation effect. This is a nonlinear effect because the only reason for the movement of the 'star' from the centre of the sample is the interaction with the accelerating beam, and this is exactly what is creating the saturation in the shift of the main lobe of this beam. The simulations also reveal a second surprising effect: the actual trajectories of the main lobe are also unexpected (see Fig. 2a). For low-power interaction,

the trajectory can be fitted to a low-order polynomial. However, as the power is increased, the main lobe is shifted strongly towards the centre of the potential induced by the 'star', only then to accelerate even faster than the original acceleration and 'escape' the gravitational potential well (as explained in the Supplementary Information). These joint effects are responsible for the saturation effect, as we explain later on. Even more importantly—these new phenomena are both nonlinear—depending on the power of the soliton 'star' and of the accelerating beam.

To understand the origin of the second effect, we have to study the experimental results more closely. The experimental data reveals the presence of tidal forces: the gravitational force exerted on the different lobes varies from one lobe to the next, owing to their different distances from the 'star' and the self-induced potential of the accelerating beam. This effect gives rise to tidal forces that deform the structure of the wavepacket as it propagates. These tidal forces arise from the potential both beams induce, although we also note the presence of a very weak self-focusing effect of the accelerating beam on itself. The tidal forces pull the lobes towards one another. Figure 2b shows the cross-sections of the beams from Fig. 1c, where the beams are superimposed such that the peaks of their main lobe are at the same position, to enable direct comparison between the structures of the beams. This reveals the effect of tidal forces on the structure of the accelerating beam. As evident from Fig. 2b, as the power of the beams is increased, the lobes are attracted

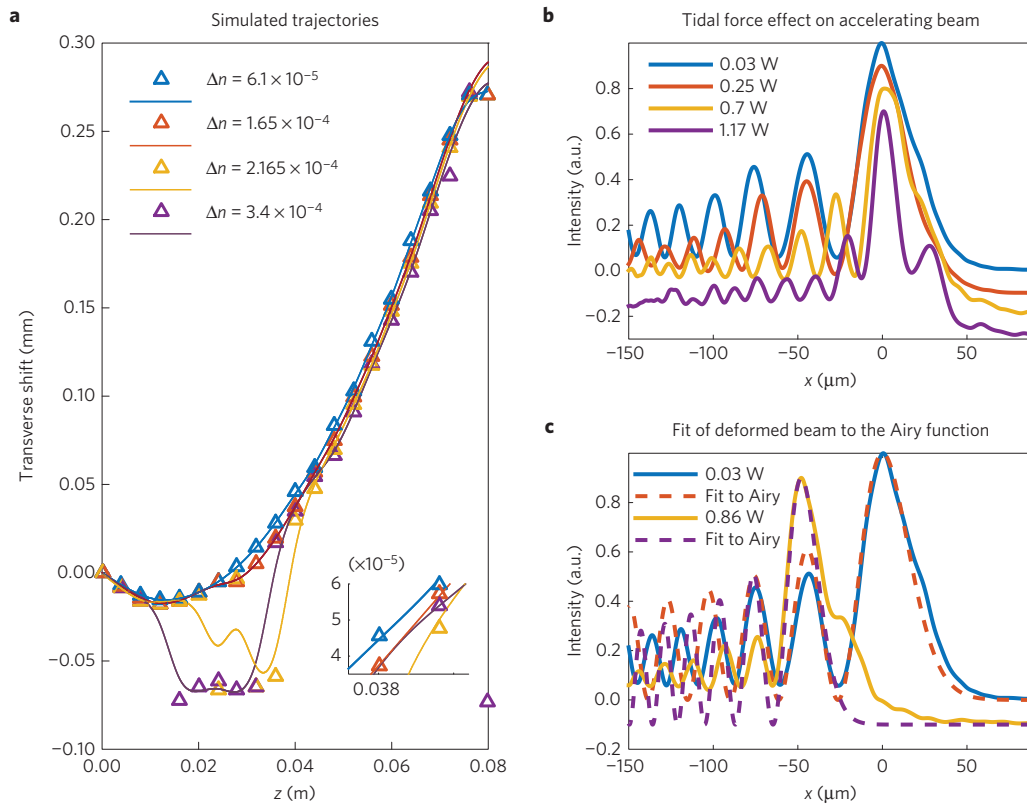


Figure 2 | Simulations and experiments showing the trajectories of the beam accelerating away from the ‘star’ and the deformation of its structure, unravelling the effect of tidal forces. **a**, Results of (2+1)D simulations showing the transverse shift (in the x direction) of the main lobe as a function of propagation distance (z). Different colours are associated with different laser power levels (interaction strengths), where the maximal change in the refractive index (of each) appears in the legend. The ratio between the power of the beams is set to 1.6% in all simulations. For low-power interaction the trajectory is a low-order polynomial (blue and red), whereas for high power (yellow and purple) the trajectories are non-trivial: starting with a strong shift towards the ‘star’ and then a fast acceleration in the counter direction (escaping away from the star) due to a nonlinear change in the refractive index and the deformation of the accelerating beam. Inset: zooming in reveals trajectories that cross each other. (The triangles represent the simulated data points.) **b**, Experimental results: 1D cross-section of the 2D accelerating beam taken along the line marked in Fig. 1b, for various laser power levels (interaction strengths) with the gravitational lensing factored out. The waveforms are shifted slightly vertically for clarity. Note that the oscillations in the structure of the accelerating beam become faster as the power is increased, owing to tidal force effects exerted by the powerful beam (the star). This beam deformation is responsible for the increase in the acceleration in the simulation shown in **a**. **c**, Experimental results showing the structure of the accelerating beam at various power levels, compared to the (linear, non-interacting) Airy function, to highlight the deformation of the accelerating beam due to the tidal forces. The deformation results in a change in the acceleration as the simulation reveals in **a**.

to one another, creating faster spatial oscillations in the structure of the accelerating beam. Our observation of the change in the width of the main lobe as a function of the power is presented in the Supplementary Information, revealing a pronounced effect of the tidal force: as the power is increased, the main lobe width decreases to almost half its width. Figure 2c shows a comparison between the structures of two accelerating beams at two different power levels. Fitting (numerically) the shape of the accelerating beam emerging from the interaction to an Airy function reveals that the oscillations of the Airy function have almost doubled their (local) frequencies, at high power. This means the beam accelerates much faster owing to the deformation of the structure of the beam (see Supplementary Information), causing the non-trivial trajectories observed in the simulation. This is a very surprising effect—the non-local nonlinearity deforms the structure of the wavepackets owing to an effect analogous to tidal forces, thus affecting the acceleration—which in itself arises from interference effects. This manifests a subtle interplay between the nonlocal nonlinearity effects on the beam and the beam acceleration, which is, in itself, a consequence of the shape of the beam. Consequently, the acceleration rate is actually an outcome of the nonlinear interaction—it depends highly on the power of the beams. This feature can also contribute to

the saturation of the gravitational lensing, as we observe in the experiment (Fig. 1d). The increase in the beam acceleration due to the deformation of the beam (caused by the tidal forces) allows the beam to accelerate faster away from the centre of the potential, overcoming the gravitational lensing.

Having observed the influence of gravitational lensing on the accelerating beam (through the trajectory change and of tidal forces which deform the beam structure), we now use GR formalism to explain the experimental observations, and attempt to also shed light on the effect of the tidal forces on the saturation observed in Fig. 1d. The gravitational lensing and tidal forces are modelled using the geodesics equation, which gives the shortest path between two points in a given curved space. This is the exact path along which light will propagate, according to Fermat’s principle. For simplicity we model the behaviour in 1D. To describe the dynamics of the accelerating wavepacket, we add an inhomogeneous force term \tilde{F} , meant to describe the natural acceleration of the beam arising from the interference effect caused by the initial conditions. The equation for the trajectories of the different lobes is:

$$\frac{d^2x}{dz^2} = \frac{1}{n} \frac{d\Delta n(x,z)}{dx} + \tilde{F}(x,z) \quad (4)$$

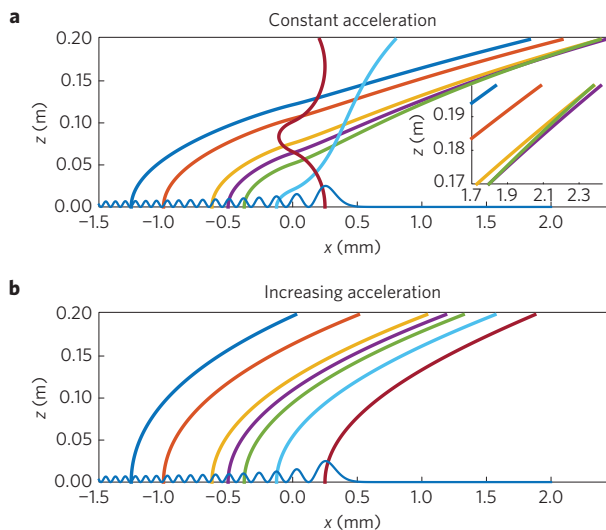


Figure 3 | Using the inhomogeneous geodesic equation to model the trajectories of the beam accelerating away from the ‘star’ and the tidal forces acting on it. **a**, Calculated trajectories that are solutions of the inhomogeneous geodesic equation (equation (4)) with the refractive index data taken from typical simulations, and where \tilde{F} is taken to be constant. Each coloured line shows the trajectory of one lobe in the beam. The lobes become closer to one another while propagating in z , which does not conform to experimental observations (Fig. 1d) and the simulations of the NSE (Fig. 2a). Inset: zooming in reveals trajectories that cross each other owing to the tidal forces. **b**, Same as **a** but when solving equation (4) $\tilde{F}(z)$ is taken to be a linear function of z . As the lobes propagate they maintain approximately the same distance from one another, conforming to the trend shown in the experiments and simulations of the NSE (Fig. 1d, Fig. 2a).

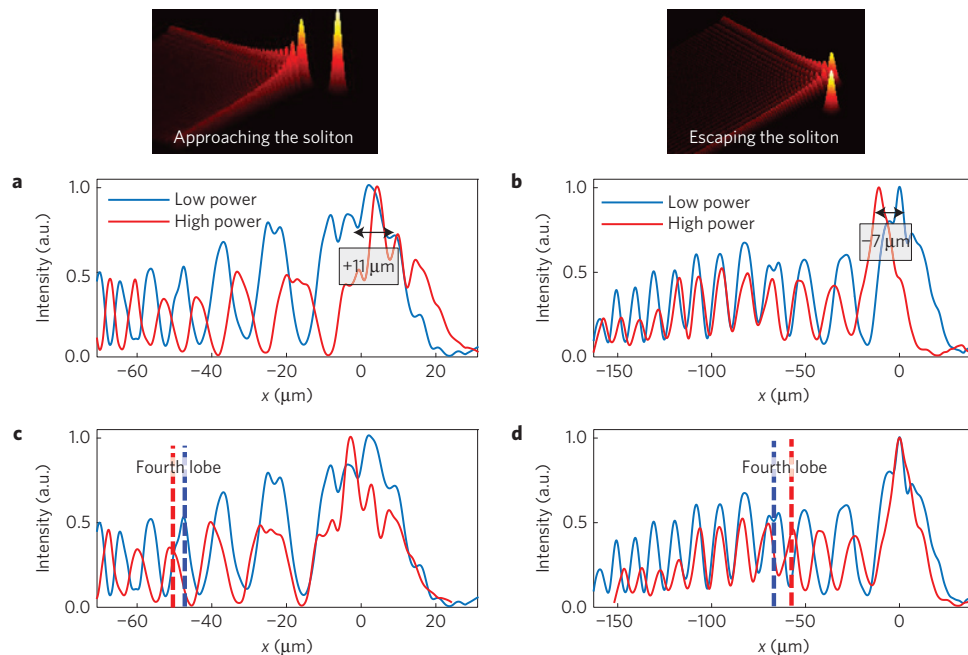


Figure 4 | Experimental observations of redshift and blueshift. **a, b**, Structure of the accelerating beam at the exit face of the lead glass sample under the influence of a change in the refractive index induced by a soliton. The main lobe is shifted owing to the interaction with the soliton, with the shift direction depending on the direction of the attracting force. For an accelerating beam approaching the soliton the main lobe is shifted towards the soliton, demonstrating the gravitational lensing effect giving a $11 \mu\text{m}$ shift (**a**). For the beam escaping the soliton there is a $-7 \mu\text{m}$ shift (**b**). **c, d**, Same as **a, b**, but with the main lobes centred at $x = 0$ to emphasize structural effects on the beam. At high power (large gravitational field), tidal forces and gravitational redshift/blueshift affect the structure of the accelerating beam: pushing the tail lobes away from the main lobe (**c**) or pulling them towards it (**d**). Illustrations of the two schemes are shown at the top of the figure, where the intensity of the powerful beam is reduced by orders of magnitude for better clarity.

The derivation of equation (4) from the geodesic equation is described in the Supplementary Information. We solve equation (4) for the trajectories of the various lobes and compare the results to the geodesics in the presence of the gravitational potential only (the homogeneous solution of equation (4)). The solutions are shown in Fig. 3a, where $\tilde{F}(x, z)$ is taken to be a constant that conforms to the experimental launch conditions (the field at $z = 0$). Similarly, the value and the structure of the refractive index change $\Delta n(x, z)$ is taken from typical simulations (specifically, 1D cross-section of the 2D refractive index profile). The lobes become closer to one another while propagating in z ; clearly, the beam is deformed and the lobes even switch positions. However, as we know from Fig. 2b, the tidal forces deform the shape of the beam, hence its spatial frequencies actually increase as the beam propagates, consequently increasing the acceleration. To model this using GR tools, we solve equation (4) with $\tilde{F}(z)$ —the inhomogeneous term—which is allowed to vary with z , to account for the acceleration change during propagation. The solutions are shown in Fig. 3b. For simplicity, $\tilde{F}(z)$ is taken to be a linear function of z and, consequently the lobes maintain approximately the same distance from one to the other as they propagate. Counterintuitively, we find that the effect of the tidal forces on the beam, modelled by a z -dependent $\tilde{F}(z)$ and which is expected to deform the beam, actually supports the shape-preserving property of the accelerating beam.

Finally, we exploit the control over the accelerating beam and conduct experiments to observe gravitational redshift and blueshift. From GR, we know that gravitational redshift occurs when light is propagating from a high gravitational potential to a lower gravitational potential (vice versa for blueshift). In the experiment, we observe interaction between a soliton (‘star’) and an accelerating beam in two different regimes: when the accelerating beam is escaping from the potential well induced by the soliton and when the accelerating beam is approaching the potential well. Following

the analogy between z (in equation (2)) and t (in equation (3)), a shift in k_z is analogous to a shift in the temporal frequency, and we can expect a change in k_z that depends on the relative motion of the wavepacket and the ‘star’ (soliton). We can use the equation from GR describing the gravitational redshift/blueshift²⁰, by replacing the gravitational potential with the change in the refractive index and the frequency with the spatial frequency (see Supplementary Information):

$$\frac{\Delta k_z}{k_z} = \Delta n(x_2) - \Delta n(x_1) \quad (5)$$

where x_1, x_2 are two positions of the main lobe (in 2D). We model the gravitational redshift/blueshift by the known relation between the spatial frequencies in the paraxial regime: $k_z = k - (k_x^2 + k_y^2)/2k$, and substitute into equation (5). In the experiment, we measure the intensity distribution of the optical beam at the exit face of the sample, which reveals the evolution of the spatial frequencies k_x, k_y due to the nonlinear effects. The blueshift and redshift are observed as a change in k_z . The gravitational redshift can even cause a stretching effect, where the lobes are pulled away from one another, as shown in Fig. 4.

To conclude, we have presented a nonlinear optical scheme to demonstrate gravitational dynamics whose description necessitates a highly nonlocal nonlinearity. We launched specifically shaped beams into a nonlocal nonlinear medium to observe, and also to affect, nonlinear gravitational effects that have thus far never been demonstrated. Perhaps even more interesting are the possibilities our system offers in the study of foundational principles combining GR and quantum mechanics. As our system is analogous to the NSE, it simulates gravity in the Newtonian limit together with quantum mechanics. Earlier studies of the NSE were strictly theoretical^{32,39}, and mostly with spherically symmetric conditions and Gaussian initial profiles of the wavefunctions. Evidently, exploring other systems with especially shaped beams has shown that unique beam profiles can reveal interesting new physics⁴⁸. It is therefore very interesting to explore this NSE system in experiments, while having control over the initial wavefunctions, as we achieved here. Clearly, it would be extremely interesting to explore this kind of setting for simulators of quantum field theory together with post-Newtonian gravity in a nonlinear theory. We believe this is actually possible and it is exactly what we plan to do next.

Received 15 April 2015; accepted 23 July 2015;
published online 31 August 2015

References

- Einstein, A. Die Grundlage der allgemeinen Relativitätstheorie. *Ann. Phys.* **354**, 769–822 (1916).
- Unruh, W. G. Experimental black-hole evaporation? *Phys. Rev. Lett.* **46**, 1351–1353 (1981).
- Lahav, O. *et al.* Realization of a sonic black hole analog in a Bose–Einstein condensate. *Phys. Rev. Lett.* **105**, 240401 (2010).
- Weinfurter, S., Tedford, E. W., Penrice, M. C. J., Unruh, W. G. & Lawrence, G. A. Measurement of stimulated Hawking emission in an analogue system. *Phys. Rev. Lett.* **106**, 021302 (2011).
- Leonhardt, U. & Piwnicki, P. Optics of nonuniformly moving media. *Phys. Rev. A* **60**, 4301–4312 (1999).
- Leonhardt, U. & Piwnicki, P. Relativistic effects of light in moving media with extremely low group velocity. *Phys. Rev. Lett.* **84**, 822–825 (2000).
- Smolyaninov, I. I. Surface plasmon toy model of a rotating black hole. *New J. Phys.* **5**, 147 (2003).
- Philbin, T. G. *et al.* Fiber-optical analog of the event horizon. *Science* **319**, 1367–1370 (2008).
- Narimanov, E. E. & Kildishev, A. V. Optical black hole: Broadband omnidirectional light absorber. *Appl. Phys. Lett.* **95**, 041106 (2009).
- Genov, D. A., Zhang, S. & Zhang, X. Mimicking celestial mechanics in metamaterials. *Nature Phys.* **5**, 687–692 (2009).
- Sheng, C., Liu, H., Wang, Y., Zhu, S. N. & Genov, D. A. Trapping light by mimicking gravitational lensing. *Nature Photon.* **7**, 902–906 (2013).
- Batz, S. & Peschel, U. Linear and nonlinear optics in curved space. *Phys. Rev. A* **78**, 043821 (2008).
- Schultheiss, V. H. *et al.* Optics in curved space. *Phys. Rev. Lett.* **105**, 143901 (2010).
- Bekenstein, R., Nemirovsky, J., Kaminer, I. & Segev, M. Shape-preserving accelerating electromagnetic wave packets in curved space. *Phys. Rev. X* **4**, 011038 (2014).
- Gorbach, A. V. & Skryabin, D. V. Light trapping in gravity-like potentials and expansion of supercontinuum spectra in photonic-crystal fibres. *Nature Photon.* **1**, 653–657 (2007).
- Batz, S. & Peschel, U. Solitons in curved space of constant curvature. *Phys. Rev. A* **81**, 053806 (2010).
- Smolyaninov, I. I. Analog of gravitational force in hyperbolic metamaterials. *Phys. Rev. A* **88**, 033843 (2013).
- Engheta, N. & Ziolkowski, R. W. *Metamaterials: Physics and Engineering Explorations* (John Wiley, 2006).
- Shalaev, V. M. Optical negative-index metamaterials. *Nature Photon.* **1**, 41–48 (2007).
- Weinberg, S. *Gravitation and Cosmology: Principles and Applications of the General Theory of Relativity* (John Wiley, 1972).
- Jacobson, T. Thermodynamics of spacetime: The Einstein equation of state. *Phys. Rev. Lett.* **75**, 1260–1263 (1995).
- Zee, A. *Einstein Gravity in a Nutshell* (Princeton Univ. Press, 2013).
- Dabby, F. W. & Whinnery, J. R. Thermal self focusing of lasers beams in lead glasses. *Appl. Phys. Lett.* **13**, 284–286 (1968).
- Rotschild, C., Cohen, O., Manela, O., Segev, M. & Carmon, T. Solitons in nonlinear media with an infinite range of nonlocality: First observation of coherent elliptic solitons and of vortex-ring solitons. *Phys. Rev. Lett.* **95**, 213904 (2005).
- Rotschild, C., Alfassi, B., Cohen, O. & Segev, M. Long-range interactions between optical solitons. *Nature Phys.* **2**, 769–774 (2006).
- Pertsch, T., Dannberg, P., Elflein, W., Bräuer, A. & Lederer, F. Optical Bloch oscillations in temperature tuned waveguide arrays. *Phys. Rev. Lett.* **83**, 4752–4755 (1999).
- Schwartz, T., Bartal, G., Fishman, S. & Segev, M. Transport and Anderson localization in disordered two-dimensional photonic lattices. *Nature* **446**, 52–55 (2007).
- Lahini, Y. *et al.* Anderson localization and nonlinearity in one-dimensional disordered photonic lattices. *Phys. Rev. Lett.* **100**, 013906 (2008).
- Plotnik, Y. *et al.* Experimental observation of optical bound states in the continuum. *Phys. Rev. Lett.* **107**, 183901 (2011).
- Rechtsman, M. C. *et al.* Photonic Floquet topological insulators. *Nature* **496**, 196–200 (2013).
- Penrose, R. On gravity’s role in quantum state reduction. *Gen. Relativ. Gravit.* **28**, 581–600 (1996).
- Moroz, I. M., Penrose, R. & Tod, P. Spherically-symmetric solutions of the Schrödinger–Newton equations. *Class. Quantum Gravity* **15**, 2733–2742 (1998).
- Tod, P. & Moroz, I. M. An analytical approach to the Schrödinger–Newton equations. *Nonlinearity* **12**, 201–216 (1999).
- Page, D. N. Classical and quantum decay of oscillations: Oscillating self-gravitating real scalar field solitons. *Phys. Rev. D* **70**, 023002 (2004).
- Guzmán, F. S. & Ureña-López, L. A. Evolution of the Schrödinger–Newton system for a self-gravitating scalar field. *Phys. Rev. D* **69**, 124033 (2004).
- Diósi, L. Notes on certain Newton gravity mechanisms of wavefunction localization and decoherence. *J. Phys. A* **40**, 2989–2995 (2007).
- Giulini, D. & Großardt, A. Centre-of-mass motion in multi-particle Schrödinger–Newton dynamics. *New J. Phys.* **16**, 075005 (2014).
- Bahrami, M., Großardt, A., Donadi, S. & Bassi, A. The Schrödinger–Newton equation and its foundations. *New J. Phys.* **16**, 115007 (2014).
- Diósi, L. Gravitation and quantum-mechanical localization of macro-objects. *Phys. Lett. A* **105**, 199–202 (1984).
- Einstein, A. Time, space, and gravitation. *Science* **51**, 8–10 (1920).
- Carlip, S. Is quantum gravity necessary? *Class. Quantum Gravity* **25**, 154010 (2008).
- Berry, M. V. & Balazs, N. L. Nonspreading wave packets. *Am. J. Phys.* **47**, 264–267 (1979).
- Siviloglou, G. A. & Christodoulides, D. N. Accelerating finite energy Airy beams. *Opt. Lett.* **32**, 979–981 (2007).
- Siviloglou, G. A., Broky, J., Dogariu, A. & Christodoulides, D. N. Observation of accelerating Airy beams. *Phys. Rev. Lett.* **99**, 213901 (2007).
- Baumgartl, J., Mazilu, M. & Dholakia, K. Optically mediated particle clearing using Airy wavepackets. *Nature Photon.* **2**, 675–678 (2008).
- Polynkin, P., Kolesik, M., Moloney, J. V., Siviloglou, G. A. & Christodoulides, D. N. Curved plasma channel generation using ultraintense air beams. *Science* **324**, 229–232 (2009).
- Schley, R. *et al.* Loss-proof self-accelerating beams and their use in non-paraxial manipulation of particles’ trajectories. *Nature Commun.* **5**, 5189 (2014).

48. Kaminer, I., Nemirovsky, J., Rechtsman, M., Bekenstein, R. & Segev, M. Self-accelerating Dirac particles and prolonging the lifetime of relativistic fermions. *Nature Phys.* **11**, 261–267 (2015).
49. Bekenstein, R. & Segev, M. Self-accelerating optical beams in highly nonlocal nonlinear media. *Opt. Express* **19**, 23706 (2011).
50. Alfassi, B., Rotschild, C., Manela, O., Segev, M. & Christodoulides, D. N. Boundary force effects exerted on solitons in highly nonlinear media. *Opt. Lett.* **32**, 154–156 (2007).

Acknowledgements

We thank A. Ori for valuable discussions that considerably contributed to our work, and A. Arie and I. Dolev for letting us use their phase masks for generating the accelerating beams. R. Bekenstein gratefully acknowledges the support of the Adams Fellowship Program of the Israel Academy of Sciences and Humanities, and a fellowship

from the Israel Ministry of Science and Technology. This research was also supported by the ICore Excellence centre 'Circle of Light' and the Binational USA-Israel Science Foundation BSF.

Author contributions

All authors contributed significantly to this work.

Additional information

Supplementary information is available in the [online version of the paper](#). Reprints and permissions information is available online at www.nature.com/reprints. Correspondence and requests for materials should be addressed to R.B.

Competing financial interests

The authors declare no competing financial interests.